Corrosion Science 79 (2014) 184–191

Contents lists available at ScienceDirect

Corrosion Science

journal homepage: www.elsevier.com/locate/corsci

Fireside corrosion degradation of ferritic alloys at 600 °C in oxy-fired conditions

T. Dudziak *, T. Hussain, N.J. Simms, A.U. Syed, J.E. Oakey

Energy Technology Centre, Cranfield University, Bedfordshire MK43 0AL, United Kingdom

ARTICLE INFO

Article history:
Received 22 June 2013
Accepted 11 November 2013
Available online 19 November 2013

Keywords:
A. Alloy
A. Steel
B. SEM
B. Energy dispersive x-ray spectroscopy
C. Atmospheric corrosion

ABSTRACT

This paper reports the results of a study carried out to investigate the effects of simulated coal/biomass combustion conditions on the fireside corrosion. The 1000 h deposit recoat exposure (5 × 200 h cycles) was carried out at 600 °C. In these tests ferritic alloys were used 15Mo3, T22, T23 and T91. Kinetics data were generated for the alloys exposed using both traditional weight change methods and metal loss measurements. The highest rate of corrosion based on EDX results occurred under D1 deposit where provoke mainly by the formation of alkali iron tri-sulphate phase.

1. Introduction

The fast growing of the modern technology demands the modern materials which can be applied at high temperatures (>600 °C) in different environments. The problem of the corrosion degradation of the materials at high temperatures is well known; boiler tubes are often subjected to fireside corrosion, where fast degradation occurs. In order to reduce the degradation of present materials, it is required to develop, a material with adequate mechanical properties and high corrosion resistance at high temperature. The power plant overall efficiency can be increased in different ways such as new methods of combustion, gasification, higher temperatures and pressures (ultra supercritical boilers), co-firing with biomass or implementation of carbon capture storage (CCS) technologies [1]. However, it is extremely important to understand the effects of these new technologies on the boiler performance to design and develop the future advanced power plants [2].

Co-firing of fuels and oxy-firing systems are both valuable methods in the development of efficient power plants and reduction in CO_2 emissions [3–6]. Biomass is classed as carbon neutral fuel, and so has zero net CO_2 emissions and the use of oxy-firing technologies for fuel combustion facilitates the post-combustion capture of CO_2 [7–9]. Oxy-firing systems are undergoing extensive research, with several system variants being considered, including: (a) hot flue gas recycle after particle removal systems; and, (b) cold flue gas recycle after acid gas removal (e.g. desulphurization) and partial water condensation. One of the greatest challenges the power generation industry faces is the excessive fireside corrosion of the heat exchangers (superheaters/reheaters). It is believed that co-firing biomass such as cereal co product (CCP) with a UK coal will release high levels of Cl and alkali metal (K), with a possible formation of KCl [2,8] on the heat exchanger surfaces. At present time alkali salts have been in focus extensively as well as chlorine-induced high-temperature corrosion caused by alkali chlorides [10,11]. Much attention of the subject is given in the literature [12,13]. A common hypothesis regarding chlorine-induced high temperature corrosion is that chlorine in the form of alkali chloride at a steel surface at temperatures higher than some.

450 °C actively increases the oxidation of the steel surface [14,15]. The process is named in some cases as "active oxidation" in which a "chlorine cycle" is assumed to be involved. This has been visualized by Vaughan et al. [14]. The role of potassium has lately become clearer through the characterisation of potassium chromate in the corrosion layer [16]. However, the exact mechanism is still not known.

Similarly, oxy-firing of such fuel blends will result in high levels of CO_2, H_2O and corrosive gases (HCl and SO_x) [6]. Both approaches (co-firing and oxy-firing) will change the combustion gas chemistry considerably and raise concerns for the life of the superheater/reheater tubes. Therefore retrofitting the existing power plants into a co-firing unit or oxy-firing without sufficient experimental data will be a huge risk.

In this paper degradation of 15Mo3 (0% Cr), T22 (~2.25% Cr), T23 (~2.5% Cr), T91 (~9% Cr) in simulated oxy-firing system (with hot flue gas recycle after a particle removal system) is presented.

* Corresponding author. Present address: Foundry Research Institute, Zakopianska 73, 30-418 Kraków, Poland. Tel.: +48 122618140; fax: +48 122618135.
E-mail address: tomasz.dudziak@iod.krakow.pl (T. Dudziak).

0010-938X/$ - see front matter © 2013 Elsevier Ltd. All rights reserved.
http://dx.doi.org/10.1016/j.corsci.2013.11.005

Table 1
Chemical composition of the materials used in fireside corrosion testing (wt%).

Alloy	Fe	C	Mn	P	S	Si	Cr	Ni	Mo	V	W	Nb	B	Al	N	Cu
15Mo3	Bal.	0.16	0.61	0.035	0.035	0.30	–	–	0.3	–	–	–	–	–	–	–
T22	Bal.	0.01	0.45	0.025	0.025	0.50	2.30	–	1.0	–	–	–	–	–	–	–
T23	Bal.	0.06	0.46	0.001	0.014	0.20	2.18	0.14	0.08	0.25	1.54	0.05	0.0023	0.001	0.0023	–
T91	Bal.	0.10	0.45	0.003	0.009	0.12	8.36	0.21	0.90	–	–	–	–	0.022	0.48	0.17

The 1000 h deposit recoat exposure (5 × 200 h cycles) was carried out at 600 °C in a controlled atmosphere furnace [17], using a gas composition to simulate the environment anticipated from a UK coal combusted with miscanthus (at 20% energy content). The microstructure and phases developed in the scales and deposits during the exposure were identified using environmental scanning electron microscopy (ESEM) with energy dispersive X-ray analysis (EDX). Finally the data generated from dimensional metrology provided quantitative information on the dependence of fireside corrosion rates on both alloy and deposit compositions.

2. Experimental procedure

2.1. Materials

In this work four alloys were used: a low carbon steel (15Mo3), two ferritic steels (T22 and T23), and one ferritic/martensitic steel (T91). The chemical composition of the materials has been measured by EDX and is shown in Table 1.

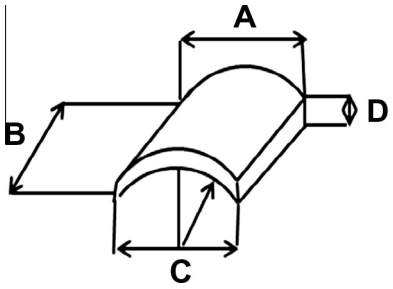

Fig. 1. Sample geometry used in this work for fireside corrosion test, (A) chord length, (B) length of the sample, (C) arc and (D) wall thickness.

Each of these materials was machined from commercial tubes in the form of tube segments. The typical dimensions of specimens were ~15 mm long with a 4 mm wall thickness. The shape of the samples used in this study is shown in Fig. 1. All surfaces of these tubes were finished to 600 grit (Ra < 0.4 μm).

2.2. Fireside exposure conditions

The fireside corrosion tests were carried out in vertical controlled atmosphere furnace (Fig. 2). Alumina lined furnaces are designed to accommodate 24 alumina crucibles (containing the samples) that sit in an alumina frame. The experimental setup to simulate oxy-firing conditions is shown in Fig. 2. The test was run using the well-established "deposit recoat" technique [2,18].

The exposure conditions for the test was set following a detailed study of the gas and deposit condition that could be produced using a common UK power station coal (Daw Mill) and biomass product (cereal co-product, CCP) available for use in UK power stations [8]. The use of these fuels at a ratio of 80:20 wt% is typical for UK power plants and has been used in this study. The gas compositions produced by these fuels in oxy-firing modes have been calculated using models that have been validated with pilot plant data [5,8]. The gas compositions have been simplified to their key active components for corrosion testing in superheater/reheater environments and shown in Table 2.

The gas mixture required to simulate the power plant environment around superheaters/reheaters was achieved by mixing gases

Table 2
Gas composition used in fireside corrosion tests.

Gas	Nominal gas composition					
	N_2 %	O_2 %	CO_2 %	H_2O %	SO_2 vpm	HCl vpm
	5.2	4	59	31	6260	1700

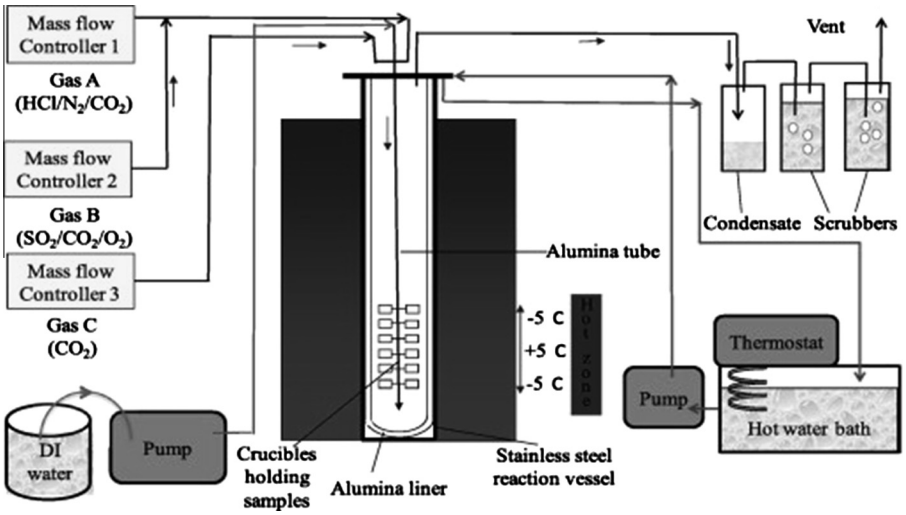

Fig. 2. Schematic diagram of a vertical controlled-atmosphere furnace setup for fireside corrosion exposures in simulated oxy-fired combustion gas used in this study.

Table 3
Chemical composition (mol%) of the deposits used in this work.

Deposit no.	Deposit composition (mol%)						
	kaolinite*	Na_2SO_4	K_2SO_4	KCl	Fe_2O_3	CaO	$CaCO_3$
D0 (bare)	–	–	–		–		
D1	–	37.5	37.5	–	25.0	–	–
D2	57.0	10.0	–	–	28.0	5.0	–
D3	57.0	5.0	5.0	–	28.0	5.0	–
D4	53.0	5.0	–	10.0	27.0	5.0	–
D5	57.0	10.0	–	–	28.0	–	5.0

* $Al_2O_3{\cdot}2SiO_2{\cdot}2H_2O$.

from three pre-mixed gas bottles using mass flow controllers. To generate the simulated oxy-fired combustion gas conditions, deionised water was supplied direct to the furnace using a peristaltic pump. The corrosive hot gases coming out from the furnace passed through an empty bottle to trap the condensate produced and then were neutralised by passing through a scrubber of NaOH solution before being vented. In this test uncoated samples (D0) and coated by one synthetic deposit (D1–D5), painted using a paint brush to give coverage of ~20 mg/cm^2. The chemical composition of the deposit used in this study is shown in Table 3.

Thus in this study in total 24 were used, 4 samples without deposit (D0) and another 20 specimens with 5 different deposits (D1–D5) listed in Table 3, these deposits can be characterised as [19]:

D0: No deposit (i.e. bare alloy surface exposed to the gas atmosphere).

D1: A standard deposit composition that is widely used in screening tests; it represents a composition of alkali–iron tri-sulphate that has been identified from many investigations as the principal cause of fireside corrosion in superheaters/reheaters in coal-fired power stations [9,20,21].

D2: The alkali–iron tri-sulphate compositions from D1 diluted with kaolinite ($Al_2O_3{\cdot}2SiO_2{\cdot}2H_2O$) to represent the clay minerals (Fe_2O_3 and CaO) usually found in coals, K_2SO_4 concentration was decreased to 0%, whereas Na_2SO_4 reduced to 10% in order to minimise aggressiveness of the deposit D2.

D3: Is similar to D2 but with equivalent addition of K_2SO_4 and Na_2SO_4 (5%) to increase aggressiveness of the deposit, other elements (kaolinite ($Al_2O_3{\cdot}2SiO_2{\cdot}2H_2O$), Fe_2O_3 and CaO) are in the same concentration as shown in D2.

D4: Is similar to D3, but with more KCl (10%) to investigate the sensitivity of corrosion damage to this change in composition as a result of biomass co-firing combined with deposit formation mechanisms. D4 does not contain K_2SO_4; however $Na2_SO_4$, Fe_2O_3 and CaO phases are in the same amounts as in D3.

D5: Is similar to D4, with more Na_2SO_4 (10% instead of 5%), lack of K_2SO_4 and KCl. Hematite (Fe_2O_3) is in similar concentration to D4, CaO was replaced by $CaCO_3$.

2.3. Methods

The samples were all cleaned before exposure in an ultrasonic bath for 20 min in Volasil followed by isopropyl alcohol (IPA). The dimensions of each sample were measured using a digital micrometer with a resolution of ±0.001 mm. Each test was designed to run for 1000 h, in order to generate accurate metal loss data for the best performing alloy(s), with five cycles of 200 h. The temperature and time for each exposure cycle was set using the furnace control unit.

Before the test each sample and each crucible was weighed individually, just before the test, crucible and the sample (with deposit) was weighed as well to calculate the amount of deposit placed on the surface of the sample.

After each cycle, the samples were unloaded from the furnace, weighed in their individual crucibles together with the oxide scale spalled from the exposed material; afterwards the individual samples were weighed alone without the crucible.

After the weight measurements, the samples were recoated with the same deposits and weighed again in their crucibles before being loaded into the furnace for another cycle. After the final cycle, samples and crucibles were weighed again, before the samples were examined.

The measurements were carried out using a digital balance with a resolution of 0.01 mg for masses <80 g. The balance was calibrated frequently using its internal calibration function and periodically with standard weights. After the weight measurements, the samples were recoated with the same deposits and weighed again in their crucibles before being loaded into the furnace for another cycle. After the final cycle, samples and crucibles were weighed again, before the samples were examined.

2.4. Sample characterisation

Following exposure, samples were mounted to protect the potentially delicate scale and deposits and then cross-sectioned perpendicular to their axes for analysis. Mounting was facilitated by a standard jig consisting of two cylindrical holes into which two pins were inserted. These pins in combination with a knife edge held the sample vertically without applying excessive force to damage the surface corrosion products. The mounting media was a 50:50 mixture of Struers Epofix low shrinkage resin and ballotini (glass spheres with diameters of ~40–70 μm). The ballotini was introduced to minimise the resin shrinkage. The samples were further treated in vacuum to reduce porosity. Cross-sectioning was carried out using as CBN type cutting wheel with an oil-based lubricant to prevent water-soluble species dissolving. The mounted samples were then sequentially ground using SiC paper and polished to 1 μm diamond paste finish using an oil-based lubricant.

The polished cross-sections of exposed materials were all measured using an image analyser to generate accurate measurements of the amount of metal remaining after the fireside corrosion test in simulated oxy-fired condition. These measurements were compared to the pre-exposure metal thickness data to produce distributions of the change in metal, resulting from the exposures. A detailed procedure for the image analysis has been reported previously [19].

3. Results and discussion

3.1. Mass change

Figs. 3A–F show a mass change data of the exposed alloys with different deposits after 1000 h of exposure at 600 °C, where D0-Fig. 3A, D1-Fig. 3B, D2-Fig. 3C, D3-Fig. 3D, D4-Fig. 3E, D5-Fig. 3F.

The presented results in Figs. 3A–F show, that the corrosion degradation of the alloys under different chemical composition of the deposits is dissimilar, thus it is not so easy to categorise which deposit is the most aggressive or harmful, which one is the undamaging or not dangerous.

The exposure of the alloys without deposit (D0) to the aggressive environmental showed that material with the highest content of Cr (T91) demonstrated the lowest mass gain, on the other hand alloy without Cr (15Mo3) showed good corrosion resistance up to 800 h, after this point some degree of spallation appeared. It is interesting to note, that two alloys T22 and T23 with 2.18 and 2.30 wt% of Cr respectively, demonstrated worst corrosion degradation that observed in 15Mo3 alloy, in mentioned alloys,

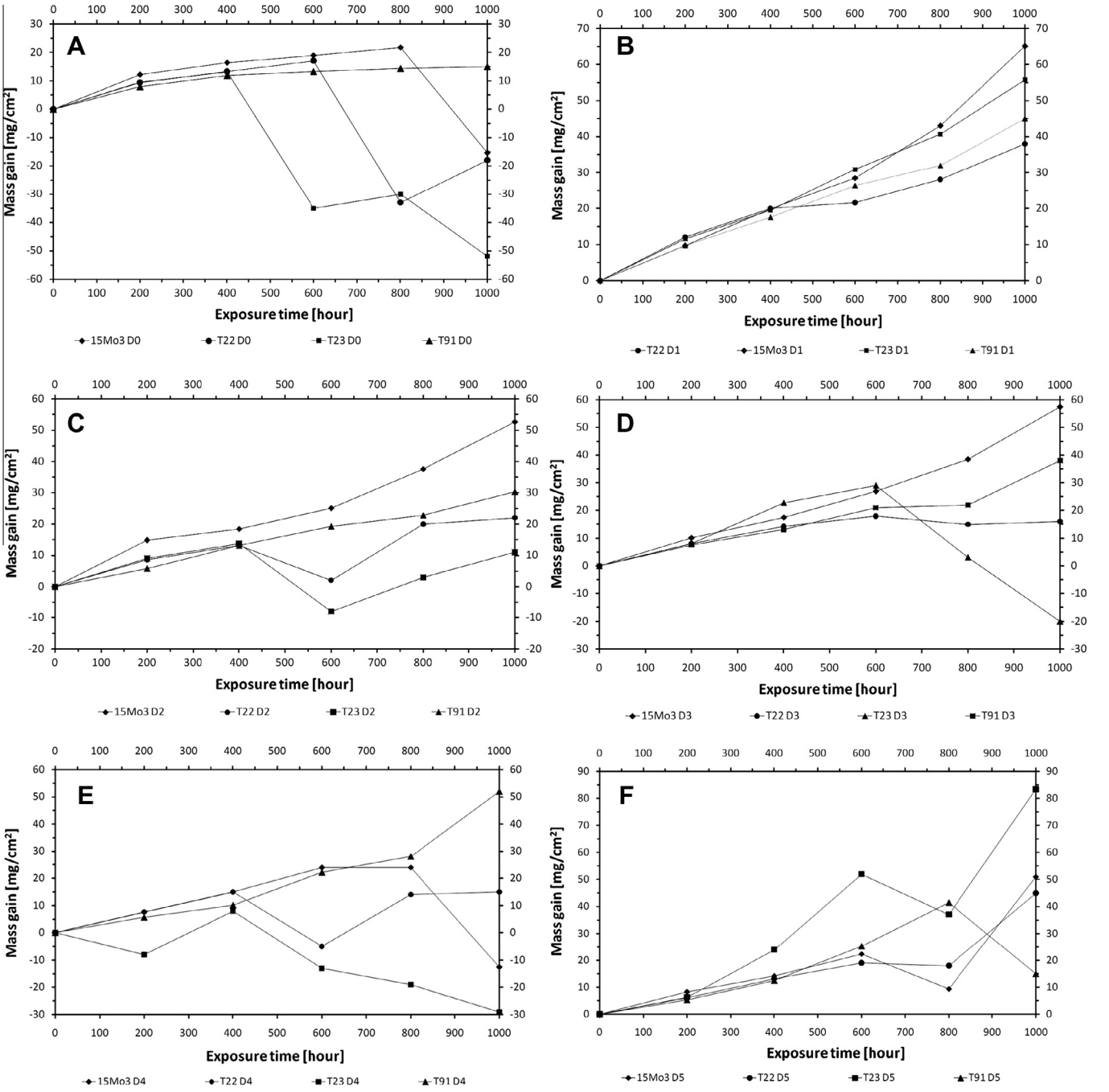

Fig. 3. Mass change data of the exposed samples after exposure at 600 °C for 1000 h in oxy-fired conditions with different deposits, (A) D0, (B) D1, (C) D2, (D) D3, (E) D4 and (F) D5.

spallation of the oxide scale became visible just after 400 h of exposure. Nevertheless, the mass change data or weight loss cannot be the only one factor determining corrosion degradation or behaviour, thus in this paper additionally metal loss data was calculated for all the exposed alloys.

The observation made by other researchers [19], suggests, that D1 is the most dangerous, and aggressive deposit used in this study. The high aggressiveness of D1 is probably due to the high concentration of Na_2SO_4 (37.5 mol%) and K_2SO_4 (37.5 mol%) in the deposit and high concentration of SO_2 in the atmosphere (6260 vpm). Based on the achieved results it can be stated that the alloys exposed to harsh environment under D1 showed relatively poor corrosion resistance in terms of mass change, ($\sim$40 mg/cm^2 for T22, $\sim$65 mg/cm^2 for 15Mo3 alloy).

Deposits D2 and D3 showed a similar corrosion influence on the exposed materials, the uppermost mass gain was achieved by the alloy with no content of Cr (15Mo3 alloy), however T91 reached slightly higher mass gain than that observed in T22 and T23 alloys.

The materials covered by D4 demonstrate, that the highest mass gain was attained by T91 alloy, with the highest content of Cr ($\sim$9 wt.%), on the other hand, the other alloys (15Mo3, T22 and T23) demonstrated some degree of spallation during the test, but mass gain of these alloys were lower than for T91.

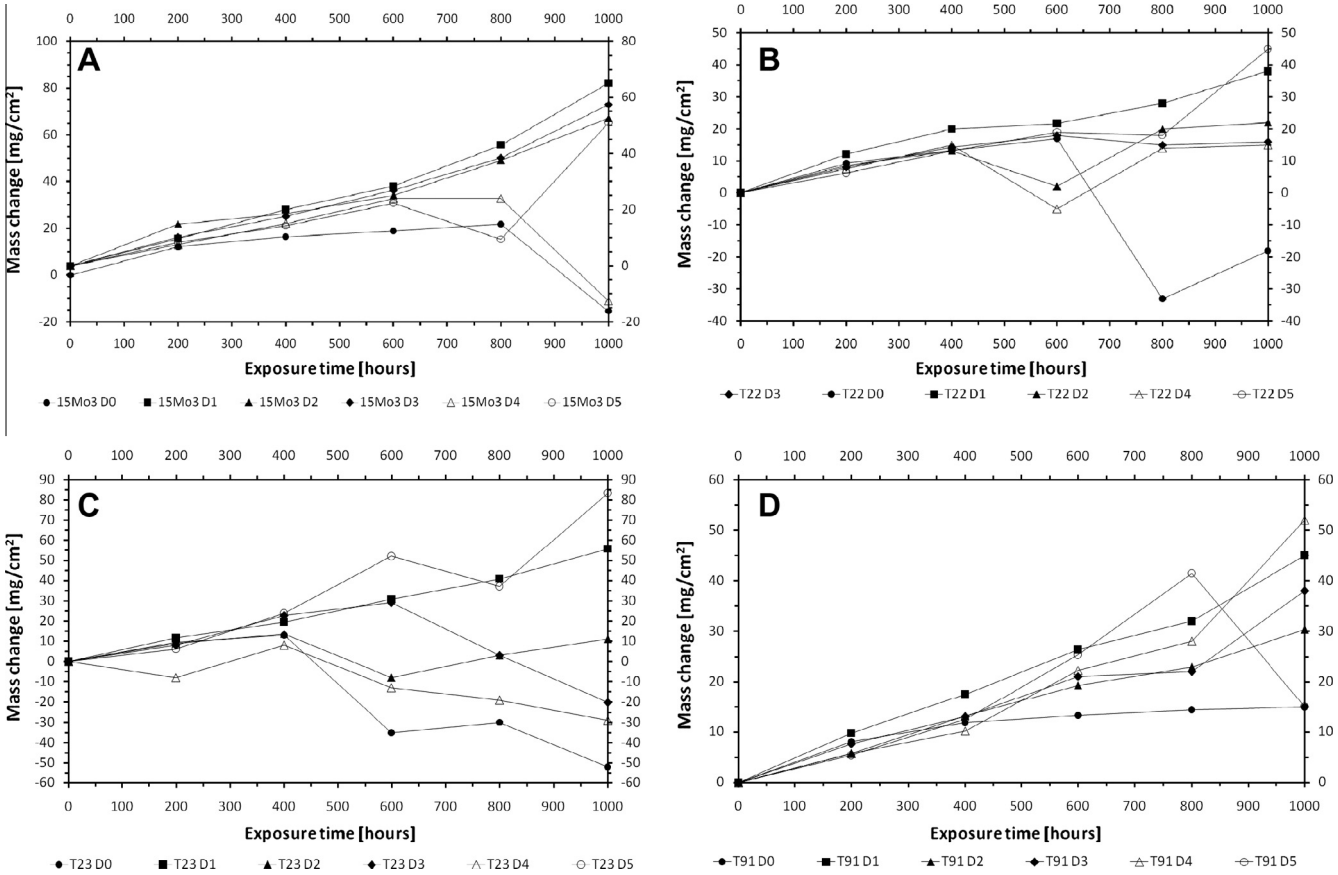

Fig. 4. Mass change data of the exposed samples with different deposits obtained after exposure at 600 °C for 1000 h in oxy-fired conditions; (A) 15Mo3, (B) T22, (C) T23, and (D) T91.

Finally D5 was more aggressive for T23 alloy where mass gain after 1000 h reached ~83 mg/cm^2, other alloys showed similar behaviour as was observed under D0–D4 deposits.

In contrast to Fig. 3, Fig. 4 shows the mass change of the same alloy with different deposits vs. time of exposure. It was observed that the exposed materials showed different behaviour; where a different deposit determines a different scenario of corrosion degradation. Therefore 15Mo3 alloy under D1 deposit showed the highest mass gain, D3, D2 and D5 showed similar behaviour where mass gain reached ~50 mg/cm^2.

The alloy T22 underwent the highest mass gain under D5 deposit where ~45 mg/cm^2 mass gain was observed, the lowest mass gain was shown by under D0 deposit, however some degree of spallation was observed.

Similar to T22 alloy, T23 materials shown the highest mass gain under D5 deposit, under D0 material lost oxide scale due to the spallation process. The D1–D4 deposits showed similar behaviour where mass gain observed was equivalent to 38, 22, 16 and 15 mg/cm^2 respectively.

The alloy with the highest concentration of Cr, demonstrate that D4 deposit accelerate mass gain of the exposed alloy, spallation was observed under D5 deposit whereas material under D0 showed lack of spallation with the lowest mass gain ~15 mg/cm^2.

3.2. Microstructural investigations

The microstructural analyses were performed on the selected materials with D1 and without deposit (D0) only, in order to show the scale changes and degradation after exposure, the results are shown in Fig. 5.

The alloys with deposit D2–D5 were investigated however ESEM images are not shown here.

The presented micrographs, clearly demonstrate that the D1 has high degree of influence on the morphologies formed during the exposure. The column A shown the materials with no deposit, the thickness of the oxide scale is similar in all exposed material this thickness is equivalent to ~90 μm, only material with no Cr content (15Mo3) showed much thicker oxide scale (~200 μm). The exposed materials with no deposit (D0) developed scale consisting: Fe_3O_4, FeO (15Mo3), Fe_3O_4, FeO + Cr (T22 alloy), Fe_3O_4, FeO + Cr + W (T23) and T91 (Fe_3O_4 + Cr, Fe–Cr spinel + S).

In contrast the materials with deposit D1 showed much thicker oxides scale (between 240 and 350 μm). Moreover, chemical composition of the formed scales covered with deposit D1 differs, from the materials without deposit.

It is suggested based on the research performed by other authors [19,21,22] The degradation of these alloys under D1 deposit is due to the formation of alkali iron tri-sulphate, the mechanism of the formation of alkali iron tri-sulphate phase is proposed below. In the first stage of the experiment SO_2 reacts with O_2 from atmosphere and O_2 derived from decomposition of H_2O.

$$H_2O \rightarrow H_{2(g)} + \frac{1}{2}O_{2(g)} \quad (1)$$

$$SO_{2(g)} + \frac{1}{2}O_{2(g)} \rightarrow SO_{3(g)} \quad (2)$$

During high temperature exposure, D1 deposit (Na_2SO_4, $K_2SO_4 + Fe_2O_3$) stars to react with formed SO_3 with the formed oxide scale on the exposed alloys according to reactions 3 and 4.

$$3Na_2SO_{4(s)} + 3SO_{3(g)} + Fe_2O_{3(s)} \rightarrow 2(Na)_3Fe(SO_4)_{3(s,l)} + 6O_{2(g)} \quad (3)$$

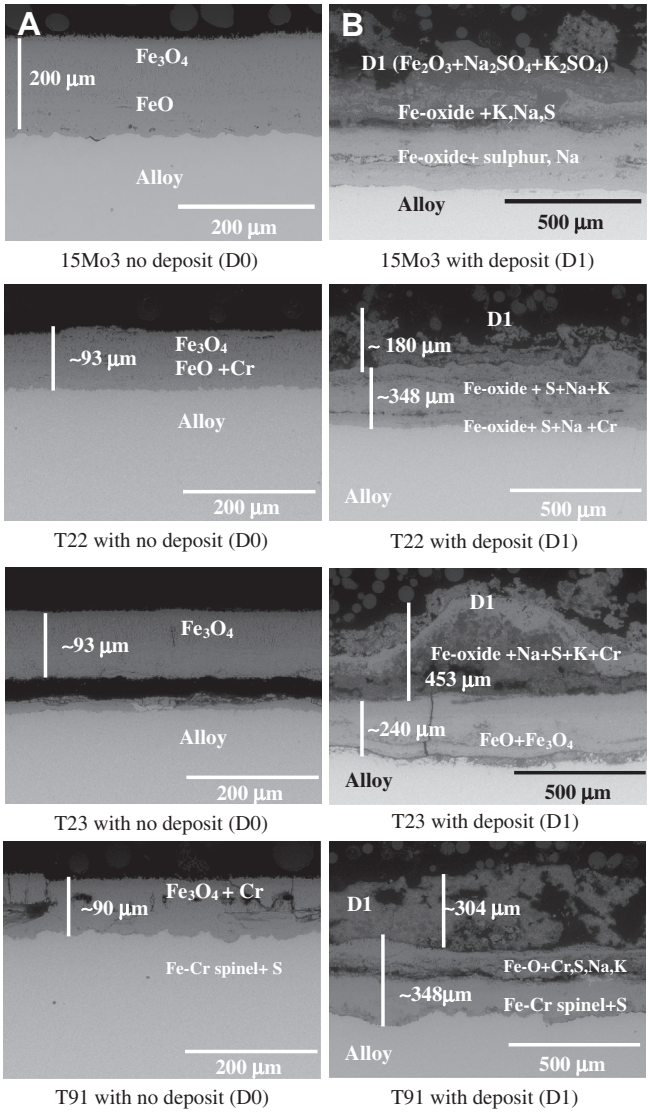

Fig. 5. BSE images of materials exposed in simulated oxy-fired combustion gases at 600 °C for 1000 h; column (A) materials without any deposit (D0), (B) materials with deposit (D1).

$$3K_2SO_{4(s)} + 3SO_{3(g)} + Fe_2O_{3(s)} \rightarrow 2(K)_3Fe(SO_4)_{3(s,l)} + 6O_{2(g)} \quad (4)$$

Above equations can be written as follows [22]:

$$SO_{3(g)} + 3(K,Na)_2SO_{4(s,l)} + Fe_2O_{3(s)} \rightarrow 2(K,Na)_3Fe(SO_4)_{3(s,l)} + 6O_{2(g)} \quad (5)$$

The formation of alkali iron tri-sulphate is predominantly a reason of the degradation of the exposed alloys under D1 deposit. Corey et al. [23] found that alkali iron tri-sulphate are stable when concentration of SO_3 decreased to specific level, tri-sulphates decompose. In this case concentration where concentration of SO_3 in flue gas reached or is higher than 250 ppm, with increasing content of SO_3, corrosive compound is more reactive and higher degradation is visible. However of SO_3 (due to the oxidation of SO_2 (reaction 2)) increased above 250 ppm, thus it can be expected that degradation due to the formation of stable alkali iron tri-sulphate is likely to occur.

Slightly lower rate of degradation was observed under D2–D5 deposits. These deposits contained more KCl, $CaCO_3$ and CaO than deposit D1. Lower corrosion degradation can be attributed due to the formation of alkali calcium tri-sulphate in D2–D4 and D5 deposits [24].

$$CaO_{(s)} + SO_{2(g)} + \frac{1}{2}O_{2(g)} \rightarrow CaSO_{4(s)} \quad (6)$$

$$CaCO_{3(s)} + SO_{2(g)} + \frac{1}{2}O_{2(g)} \rightarrow CaSO_{4(s)} + CO_{2(g)} \quad (7)$$

Further $CaSO_4$ reacts with Na_2SO_4 according to reaction below:

$$2CaSO_{4(s)} + Na_2SO_{4(s)} \rightarrow Na_2Ca_2(SO_4)_{3(s)} \quad (8)$$

The formed compound alkali calcium tri-sulphate is less corrosive than $K_3Fe(SO_4)_3$ or $Na_3Fe(SO_4)_3$, thus materials covered by deposits D2–D5 showed lower corrosion degradation, than that covered by D1 [16].

In addition according to thermodynamical calculations [25] it can be assumed the formation of volatile chlorides. At high temperatures Cl_2 in the presence of water vapour reacts with water to produce HCl. In this work, experiment was performed at 600 °C, thus accelerated corrosion due to the Cl_2 presence as well as presence of HCl needs to be considered. During the test, Cl_2 or HCl diffuses through a porous oxide scale and reach the substrate. The Fe based alloy can react with HCl/Cl_2 to formed Fe–Cl compound in the middle of the oxide scale, or nearby oxide scale substrate interface.

$$Fe_{(s)} + Cl_{2(g)} \rightarrow FeCl_{2(s)} \quad (9)$$

Grabke et al. [26] and other researchers [11,13,15] indicated that the formation of Fe–Cl phases need to be considered because Gibbs free energy formation of metal chlorides is strongly negative, also at the low oxygen partial pressure which exists make metal chloride more stable than the oxide. In contrast, on the oxide scale atmosphere interface, volatility of Fe–Cl is very high, because partial pressure of oxygen is higher than that within the oxide scale, thus Fe–Cl phase become unstable and reacts with oxygen from the decomposition of H_2O at high temperature. The Fe–Cl phase reacts to form magnetite phase according to the reaction 10:

$$3FeCl_{2(s)} + 2O_{2(g)} \rightarrow Fe_3O_{4(s)} + 3Cl_{2(g)} \quad (10)$$

This oxide is a non-protective where voids and holes always form, due to the fast diffusion process, thus due to the fast mass transport, from the atmosphere and from the substrate. The formation of magnetite close the loop, from this point, relapsed Cl_2 diffuses inwards through the pores and voids in order to react with the metal to form metal chlorides. Thus, a cycle is formed that provides a continuous transport of metal away from the metal surface towards higher oxygen partial pressure; the rate of this phenomena depends on the rate of diffusion of chlorine between the gas phase and the metal. Gas diffusion through the scale is believed to be the rate-controlling step in the corrosion process [18].

In overall, poor fireside corrosion resistance of the materials, exposed in this work is mainly related to the low Cr content, according to the work performed by Paul and Clark [22] at least 30% of Cr needs to be use in order to retard the formation of non-protective Fe-oxides, and provoke to the formation of Cr_2O_3 oxide or Fe–Cr spinel.

3.3. Dimensional metrology

The polished cross-sections were all measured using an image analyser to generate accurate measurements of the amount of metal remaining after the corrosion tests; these measurements were compared to the pre-exposure metal thickness data to produce distributions of the change in metal resulting from the exposures. Acquiring metal loss data of metal loss is crucial for the reliability of the power plant. This technique uses a digital image analyser, by comparing sample dimensions before (reference sample/unexposed) and after exposure, the apparent change in metal (metal loss) can be calculated. These data sets can then be re-ordered

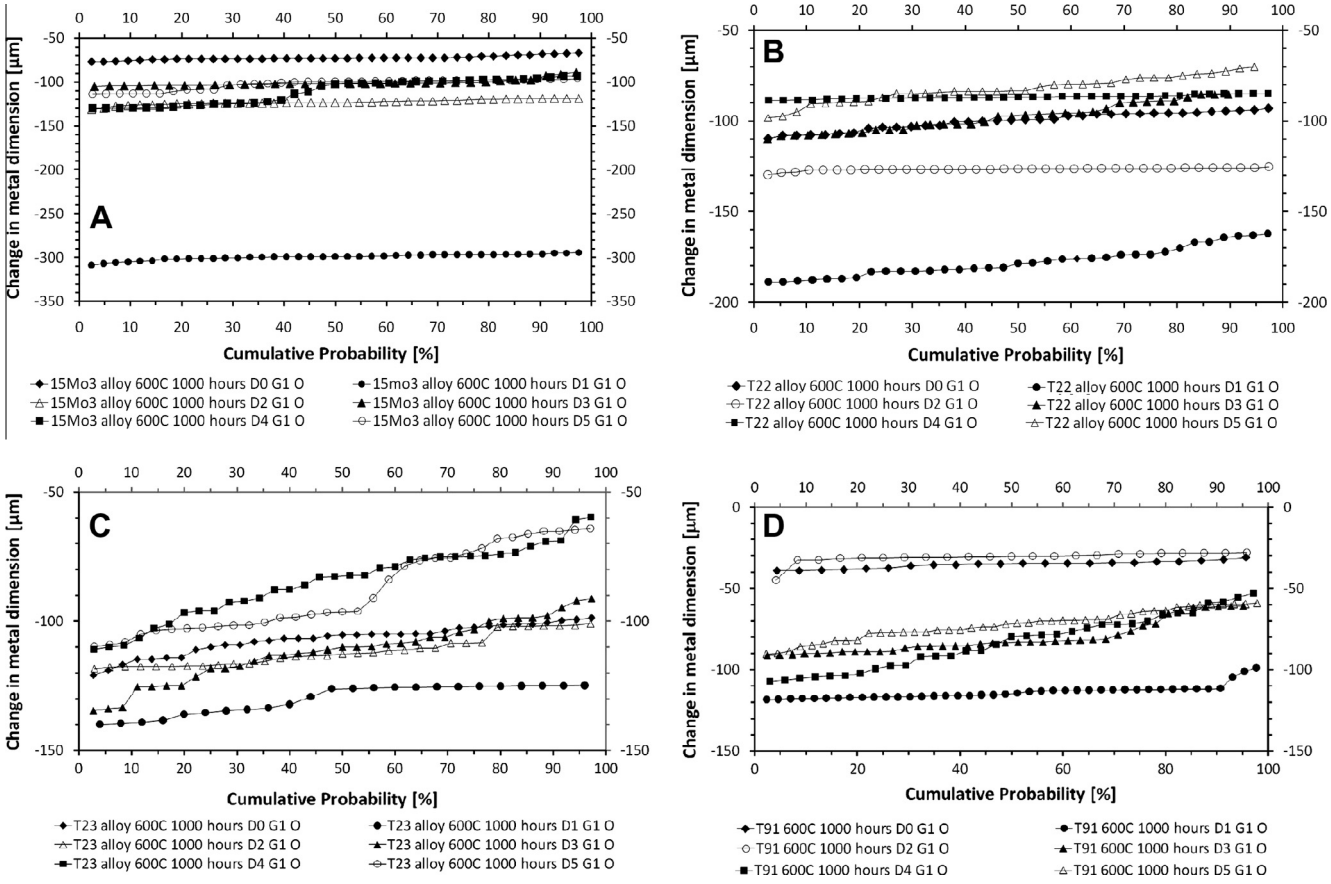

Fig. 6. Dimensional metrology of the samples exposed at 600 °C, (A) 15Mo3, (B) T22, (C) T23 and (D) T91.

(from greatest to least metal loss) and corrected for calibration differences (using data from reference samples). The processed data can then be plotted as a change in metal vs. cumulative probability; effectively, this type of plot indicates the probability (e.g. 4%) of a certain degree of damage being observed. The image analyser is connected with an optical microscope. Fig. 6 illustrates the change in metal thickness (µm) vs. cumulative probability (%) for all the alloys exposed in this work with and without deposit.

The illustrated change in the metal loss vs. cumulative probability in Fig. 6, confirms that T91 alloy, showed lower good metal consumption than the exposed alloys with lower concentration of Cr, especially under D0 and D2. The influence of the other deposits examined in this study showed similar behaviour of T91 as seen in low Cr alloys (T22, T23 and 15Mo3), where metal loss was comparable.

Additionally, in terms of kinetic changes T91 alloy showed similar behaviour as the other alloys where spallation of the oxide scale occurred. The alloys covered by deposit D1 showed the highest degree of metal loss, compared with the other deposits used in this work. The diluted version of D1 deposit, deposit D2 also showed a high degree of aggressiveness. The moderate level of corrosion degradation was achieved by D3, D4 and D5; these deposits contained more KCl, $CaCO_3$ and CaO than D1 and D2, were used to simulated fast growing biomass deposit (willow, olive waste and miscanthus). Thus the results presented here, suggest that in some cases, the alloys without deposit (D0) showed a higher or similar degradation rate to that with deposit D3–D5.

4. Conclusions

This paper reported the results of a study carried out to investigate the effects of simulated coal/biomass combustion conditions on the fireside corrosion of superheater/reheater materials. Four different materials were included in this work to investigate the effect of different alloy compositions: 15Mo3 (0% Cr), T22 (~2.25% of Cr), T23 (~2.5% Cr), T91 (~9% Cr), the following conclusions can be written:

1. All the exposed alloys in this work and coated with deposit (D1–D5) showed some degree of degradation.
2. Under D1 deposit the formation alkali iron tri-sulphate phase was found, high rate o metal degradation was found.
3. Slightly lower corrosion degradation under D2–D5, was observed, mainly due to the lower amount of Na_2SO_4 and K_2SO_4 in the deposit,
4. Higher level of KCl, $CaCO_3$ and CaO as well as K_2SO_4 and Na_2SO_4 initiate corrosion degradation.
5. It is suggested through this research that the formation of alkali calcium tri-sulphate was found under deposits with CaO and $CaCO_3$.
6. The formation of volatile FeCl phase/s cannot be neglected in this research.

Acknowledgments

Authors like to acknowledge the support of The Energy Programme, which is a Research Councils UK cross council initiative led by EPSRC and contributed to by ESRC, NERC, BBSRC and STFC, and specifically the Supergen initiative (Grants GR/S86334/01 and EP/F029748) and the following companies; Alstom Power Ltd., Doosan Babcock, E. ON, National Physical Laboratory, Praxair Surface Technologies Ltd., QinetiQ, Rolls-Royce plc, RWE npower, Siemens Industrial Turbomachinery Ltd. and Tata Steel, for their valuable contributions to the project.

References

[1] Advanced Power Plant Using High Efficiency Boiler/Turbine, Best Practice Brochure, Carbon Abatement Technologies Programme, 2006.
[2] B.-J. Skrifvars, R. Backmana, M. Hupaa, K. Salmenoja, E. Vakkilainen, Corrosion of superheater steel materials under alkali salt deposits Part 1: The effect of salt deposit composition and temperature, Corros. Sci. 50 (2008) 1274–1282.
[3] P. Dechamps, The EU Research Strategy Towards Zero Emission Fossil Fuel Power Plants, in: J. Lecomte-Beckers, M. Carton, F. Schubert, P.J. Ennis, Materials for Advanced Power Engineering (2006) 25–40.
[4] M. Farley, Clean Coal Technologies for power generation, in: A. Strang, W.M. Banks, G.M. McColvin, J.E. Oakey, R.W. Vanstone, Parsons 2007: Power Generation in an Era of Climate Change, IOM, 2007, pp. 335–342.
[5] N.J. Simms, P.J. Kilgallon, J.E. Oakey, Fireside issues in advanced power generation systems, Mater. Sci. Eng. Energy Syst. 2 (2007) 154–160.
[6] B. Bordenet, F. Kluger, Thermodynamic modelling of the corrosive deposits in oxy-fuel fired boiler, Mater. Sci. Forum 261 (2008) 595–598.
[7] JE. Oakey, LW. Pinder, R. Vanstone, M. Henderson, S. Osgerby, Review of status of advanced materials for power generation, COAL 1509 (2003).
[8] N.J. Simms, P.J. Kilgallon, J.E. Oakey, Degradation of heat exchanger materials under biomass co-firing conditions, Mater. High Temp. 24 (2007) 333–342.
[9] J. Stringer, I.G. Wright, Current limitations of high-temperature alloys in practical applications, Oxid. Met. 44 (1995) 265–308.
[10] PA. Alexander, Laboratory studies of the effects of sulfates and chlorides on the oxidation of superheater alloys, in: R. Johnson, D.J. Littler (Eds.), The Mechanisms of Corrosion by Fuel Impurities, Butterworth, 1963.
[11] HJ. Grabke, Fundamental mechanisms of the attack of chlorine, HCl and chlorides on steel and high temperature alloys in the temperature range 400–900 °C, in: RW. Bryers (Ed.), Incinerating Municipaland Industrial Waste, Hemisphere Publishing Corporation, 1989, p. 161.
[12] J. Petterson, C. Petterson, H. Asteman, J.-E. Svensson, L.G. Johansson, A pilot-plant study of the effect of alkali salts on the initial stages of the high temperature corrosion of alloy 304L, Mater. Sci. Forum 461–464 (2004) 965–972.
[13] H.P. Nielsen, F. Frandsen, K. Dam-Johansen, L. Baxter, The implications of chlorine-associated corrosion on the operation of biomass-fired boilers, Progr. Energy Combust. Sci. 26 (2000) 283–298.
[14] D.A. Vaughan, H.H. Krause, W.D. Boyd, Chloride corrosion and its inhibition in refuse firing, in: Proceedings of The International Conference on Ash Deposits and Corrosion from Impurities in Combustion Gases, Henniker, New Hampshire, USA, 1977.
[15] H.J. Grabke, E. Reese, M. Spiegel, The effects of chlorides, hydrogen chloride and sulphur dioxide in the oxidation of steels below deposits, Corros. Sci. 37 (7) (1995) 1023–1043.
[16] A. Karlsson, P.J. Möller, V. Johansen, Iron steel corrosion in a system of O_2, SO_2 and alkali chloride. The formation of low melting point salt mixtures, Corros. Sci. 30 (1990) 153.
[17] SRJ. Saunders, in: H.J. Grabke, D.B. Meadowcroft (Eds.), Guidelines for methods 615 of testing and research in high temperature corrosion, The Institute of Metals, London, 1995.
[18] T. Hussain, T. Dudziak, N.J. Simms, J.R. Nicholls, Fireside corrosion behaviour of HVOF & plasma sprayed coatings in advanced coal/biomass co-fired power plants, J. Therm. Spray Technol. 22 (2012) 797–807.
[19] A.U. Syed, N.J. Simms, J.E. Oakey, Fireside corrosion of super-heaters: effects of air and oxy-firing of coal and biomass, Fuel 101 (2012) 62–73.
[20] N.J. Simms, P.J. Kilgallon, J.E. Oakey, Fireside issues in advanced power generation systems, Mater. Sci. Eng. Energy Syst. 2 (2007) 154–160.
[21] K. Natesan, A. Purohit, D.L. Rink, Coal-ash corrosion of alloys for combustion 628 power plants, in: Presented at Fossil Energy Conference, 2003.
[22] L. Paul, G. Clark, Coal ash corrosion resistance of new chromium and chromium silicon alloys, in: Presented at NACE Presented at Corrosion 2005 Conference (Paper no. 05453).
[23] R.C. Corey, B.J. Cross, W.T. Reid, Trans. ASME 67 (1945) 289.
[24] A. Rahmel, Mechanism of Corrosion by Fuel Impurities, Butterworths, London, 1963.
[25] A.J.B. Cutler, E. Raask, External corrosion in coal-fired boilers: assessment from laboratory data, Corrosion Science, vol. 41, Pergamon Press, 1981.
[26] H.J. Grabke, E. Reese, M. Spiegel, The effects of chloride, and sulphur dioxide in the oxidation of steels below deposits, Corros. Sci. 7 (1995) 1023–1043.